Journal of Inorganic and Organometallic Polymers and Materials (2022) 32:854–863
https://doi.org/10.1007/s10904-021-02212-w

Cellulose-Based Hybrid Nanoarchitectonics with Silver Nanoparticles: Characterization and Antimicrobial Potency

E. S. Madivoli[1] · P. G. Kareru[1] · A. N. Gachanja[1] · D. S. Makhanu[2] · S. M. Mugo[3]

Received: 7 September 2021 / Accepted: 19 December 2021 / Published online: 24 January 2022

Abstract
In this study, 2,2,6,6-Tetramethylpiperidin-1-yl oxyl (TEMPO) oxidized cellulose nanofibrils (CNFs) decorated with silver nanoparticles (AgNPs) have been demonstrated as hybrid framework for microorganism inhibition. The AgNPs@CNFs nanocomposite have been characterized by fourier transform infrared spectrophotometer, X-ray diffractometer, differential scanning calorimeter and thermal gravimetric analyser. The morphology, size and zeta potential of the nanocomposite was evaluated using transmission electron microscopy and dynamic light scattering while the antimicrobial activity was evaluated using disc diffusion assay. The reduction of silver ions in the presence of CNF was a function of time as the intensity of the SPR band increased with increase in reaction time. The AgNPs@CNF composite had a higher thermal stability and fiber length between 50 and 400 nm, while the average size, polydispersibility index and zeta potential were found to be 97.8 ± 17.9 nm, 0.5393 ± 0.09 and -23.78 ± 3.71 (mV) respectively. The zone of inhibition of the nanocomposite against *Escherichia coli*, *Proteus mirabilis*, *Pseudomonas aeruginosa*, *Bacillus subtilis*, *Staphylococcus aureus*, *Candida albicans* were found to be 8.7 ± 0.6, 10.7 ± 0.6, 8 ± 1, 11 ± 1, 10.7 ± 0.6, 10.3 ± 0.6 mm. The AgNPs@CNFs nanocomposite is a good candidate for developing antimicrobial wound dressing that can inhibit the growth of microorganism.

Keywords Cellulose nanofibrils · Silver nanoparticles · Nanocomposite · Antimicrobial activity

1 Introduction

Cellulose nanofibrils (CNFs) are biodegradable, biocompatible, abundant, and easily functionalized nanomaterials finding applications in numerous fields including packaging material, batteries and medical wound dressing [1]. Wound dressings that are multifunctional such as providing physical barrier while being antimicrobial and release therapeutic agents are desirable [2–5]. Imparting antimicrobial activity to CNFs can be achieved through surface modification in which an antimicrobial moiety is anchored onto the fibers. The plethora of hydroxyl groups on CNFs surface can be modified to aldehydes [6], carboxylic acids [7] and amines [8], using well known facile chemistry reactions, thereby achieving a material with diverse functionalities and applications. Moreover, the CNFs can easily be grafted with a wide range of compounds such as proteins, polymers [9], metallic nanoparticles [10–13] and antibiotics [3]. When cellulose reacts with periodate under acidic or alkaline conditions at elevated temperature, the C_2 and C_3 bond in the glucopyranose ring are cleaved leading to the formation of 2,3 dialdehyde cellulose (DAC) making the fibrils prone to further functionalization into carboxylic acids, alcohols, imines and sulfonated cellulose (Fig. 1) [6, 14–16]. Similarly, the C_6 of cellulose can readily be converted to carboxylic group via TEMPO mediated oxidation lending the CNF surface to be chemically active with increased affinity to metallic ions [4, 7, 8, 17].

The crosslinking property of DAC has been utilized to make TEMPO/periodate oxidized films covered with polyvinylamine composite with bactericide effect for wound dressing applications. The TEMPO oxidation of cellulose followed by subsequent periodate oxidation yielded crosslinked films that had better antimicrobial activity as

✉ E. S. Madivoli
edwin.madivoli@jkuat.ac.ke

[1] Chemistry Department, Jomo Kenyatta University of Agriculture and Technology, P.O Box 62 000-00200, Nairobi, Kenya

[2] Department of Biological & Physical Sciences, Karatina University, P.O Box 1957-10101, Karatina, Kenya

[3] Chemistry Department, McEwan University, 10700-104 Avenue, Edmonton, AB T5J 4S2, Canada

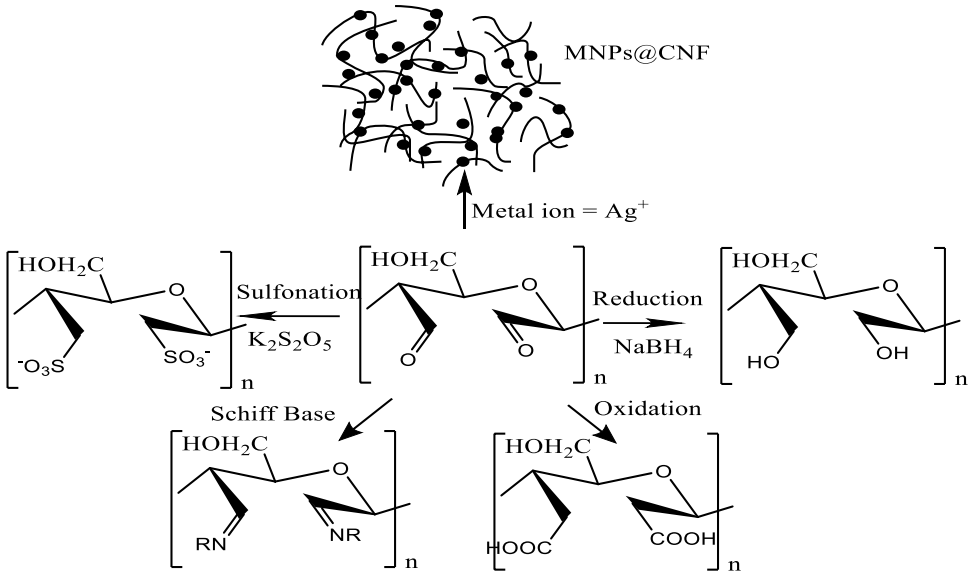

Fig. 1 Preferential surface modification of dialdehyde CNFs

fewer bacteria developed on these films as compared to films obtained after TEMPO oxidation only [18]. Oxidized cellulose in the form of gels have also been effectively applied as cationic detoxification enterosorbent agents [4]. Working on the basis of cation exchange, the technology has been applied for environmental remediation, for example in removal of heavy metals from ecosystems [19, 20]. Dialdehyde cellulose (DAC), on the other, has also been used to reduce silver ions in solution to silver nanoparticles (AgNPs) thereby imparting antimicrobial properties to the resulting composite materials [2, 11, 21, 22]. The In-situ synthesized AgNPs had the advantage of having diameters less than 100 nm as their growth was controlled by DAC which functioned as a stabilizer and capping agent, thereby preventing their agglomeration upon drying [20]. The AgNPs@CNFs composite films have the advantage of being biocompatible, biodegradable, environmental friendly and they could inhibit the growth of microorganism [9, 21]. The current study demonstrates the ability of CNF to efficiently grow AgNPs in solution to form AgNPs@CNFs composite without the need of reducing agents. Native cellulose was modified by reaction with (2,2,6,6-Tetramethylpiperidin-1-yl)-oxyl (TEMPO) to introduce carboxyl group at C_6 followed by subsequent oxidation using potassium periodate to introduce carbonyl groups at C_2 and C_3. The dialdehyde CNFs mediated in-situ reduction of Ag ions to form AgNPs@CNFs composite films whose surface morphology, thermal stability and functional groups were studied. The antimicrobial activity of AgNPs@CNFs nanocomposite films was evaluated using disc diffusion assay against *Escherichia coli*, *Proteus mirabilis*, *Pseudomonas aeruginosa*, *Bacillus subtilis, Staphylococcus aureus* and the fungi *Candida albicans*.

2 Materials and Methods

2.1 Materials

Hydrochloric acid, acetic acid (≥ 99%), hydrogen peroxide (30 wt%), (2,2,6,6-tetramethylpiperidine-1-yl)oxyl (TEMPO), potassium periodate, sodium hypochlorite (10–15%), sodium bromide (≥ 99%) and sodium hydroxide (≥ 98%) all of ACS grade were purchased from Sigma Aldrich, Saint Galen, Switzerland.

2.2 TEMPO Periodate Oxidation of Cellulose

Oryza sativa husks was used to isolate microcrystalline cellulose (MCC) according to a that we have reported in literature [23–25]. After isolation of MCC using peracetic acid (CH_3COOH:H_2O_2 5:1), TEMPO oxidized cellulose nanofibrils were prepared by dispersing MCC (2 g) in 50 mL deionized water containing TEMPO (0.32 mmol) and sodium bromide (5.0 mmol). To this solution, 0.05 mmol NaClO solution were then added at room temperature and changes in pH of the solution controlled by dropwise addition of NaOH (0.5 M) solution to maintain the solution pH at 10 [20]. After 3 h, the reaction was stopped by addition of ethanol and centrifuging several times to remove inorganics salts and TEMPO by washing with distilled water to neutral pH [7]. This was then followed by addition of HCl (2 M) to the CNF suspension to convert the C_6COONa groups to C_6COOH groups, washed to neutral pH and drying in an oven to constant weight [26]. After drying, the CNFs were further subjected to periodate oxidation using KIO_4 [16]. To introduce the

C=O functional groups on C_2 and C_3 of CNF, 1.0 g of the fibrils were resuspended in 50 ml MilliQ water and disintegrated using an ultrasonic disintegrator. Next 8.86 mmol KCl and 5.21 mmol of KIO_4 were added to the wet pulp. The reaction vessel was then wrapped in aluminum foil to prevent entry of light and the oxidation performed at 50 °C for 16 h. This was followed by addition of ethanol at the and washing with water to remove impurities and drying to constant weight [6, 16, 21, 27].

2.3 Preparation of AgNPs in CNFs Suspension

To prepare AgNPs@CNFs composite, 2 g of CNFs was dispersed in 50 mL of 100 mM silver nitrate aqueous solution heated at 80 °C in the dark for 2 h to allow reduction of Ag ions by carbonyl groups present in CNF [13]. Aliquots of 3.5 mL were subsequently drawn at time intervals and the solution measured using Shimadzu 1800 UV–Vis spectrophotometer (Shimadzu, Japan). The reduction of silver ions led to the formation of AgNPs in the CNFs dispersion confirmed through observation of SPR peak of AgNPs [2, 20, 21].

2.4 Characterization of Cellulose Nanocomposite

The oxidation of cellulose was observed through identification of new functional groups introduced in the composite using a Bruker Tensor II FT-IR spectrophotometer model (Bruker, Ettlingen, Germany) using pressed KBr pellets prepared under a pressure of 75 kPa for 3 min [28]. A STOE STADIP P X-ray Powder Diffraction System (STOE & Cie GmbH, Darmstadt, Germany) equipped with a copper tube operating at 40 kV and 40 mA irradiating the sample with a monochromatic CuKα radiation (0.1542 nm) was used to observed crystallinity changes. The crystal size and crystallinity index (CI_{XRD}) were obtained using the Scherrer equation and the peak height method respectively [24, 29]. A Bechman Coulter DelsaMax pro Dynamic light scattering analyzer (Indianapolis, United States) was used to determine the zeta potential, hydrodynamic size and the polydispersibility index of the composites. The thermal profile of the composite was evaluated using a Mettler Toledo TGA/DSC 3 + (Mettler-Toledo GmbH, Switzerland) by heating 10 mg samples from 25 to 500 °C at 10 °C min^{-1} and subsequent cooling to 25 °C. A Tescan Mira3 LM Field Emission Scanning electron microscope (FE-SEM) operated at an accelerating voltage of 3 kV was used to evaluate the surface morphology [23, 30, 31]. TEM micrographs were acquired on a Tecnai G2 Spirit (Thermo Fisher Scientific, Oregon USA) operated at 120 kV after suspending the composite in deionized water and drop casting on 300 mesh carbon films (Electron microscopy science, CF300-CU).

2.5 Disc Diffusion Assay for Antimicrobial Activity

The antimicrobial potency of the AgNPs@CNFs nanocomposite against *E. coli*, *P. mirabilis*, *P. aeruginosa*, *B. subtilis, S. aureus* and the fungal pathogens *C. albicans* was evaluated using Kirby–Bauer Disk Diffusion Assay. A sterile cotton swab was used to spread the bacteria strains on the Mueller–Hinton agar (MHA) (Merck, Germany). Sterile blank antimicrobial susceptibility disk was used in the test. The nanocomposite solution were loaded on sterile disk, dried and place on the agar plates which were then incubate 37 °C for 24 h [22, 32].

3 Results and Discussion

3.1 Synthesis of AgNPs@CNFs

The growth of AgNPs on CNF was studied real time by use of UV–Vis spectroscopy and the results are depicted in Fig. 2.

As it can be observed from Figs. 2 and 3, synthesis of AgNPs was confirmed by the presence of AgNPs plasmon resonance peak which has previously been reported as a qualitative indicator of the presence of the AgNPs in solution. As the reaction progressed, a spectral feature gradually formed at 412 nm as a function of time suggesting a continuous growth of the nanoparticles and a change in color of the solution from colorless to brick red were the initial indicators of the presence of AgNPs [20–22]. The reduction of Ag ions to AgNPs in solution is as a result of presence of

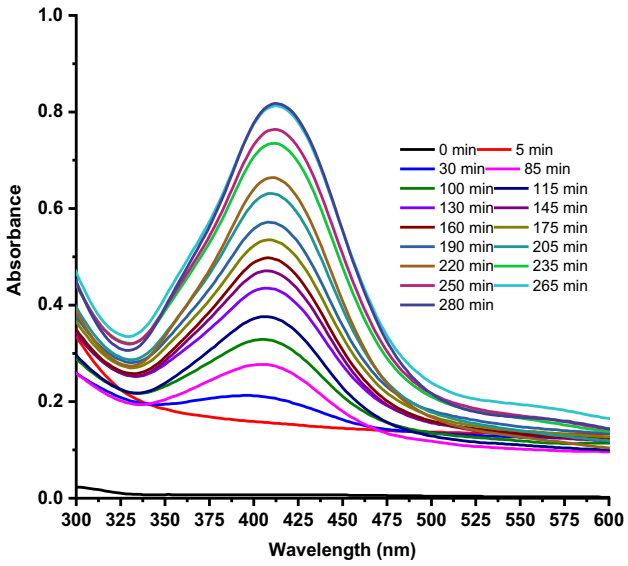

Fig. 2 UV–Vis spectra tracking formation AgNPs synthesized from 0.1 M $AgNO_3$ using CNFs

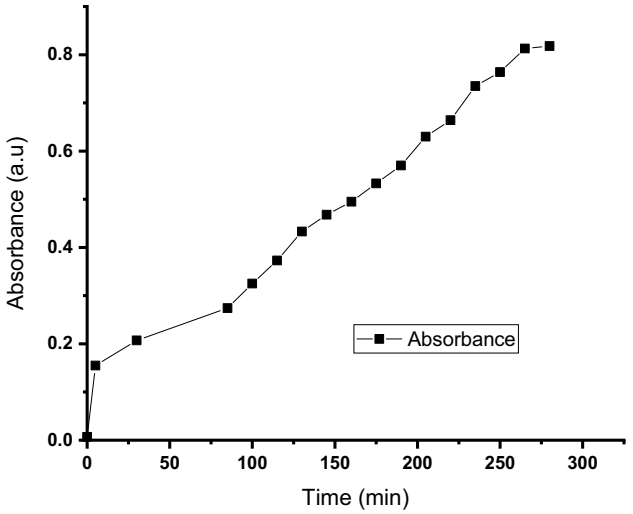

Fig. 3 A graph of absorbance against time for the synthesis of AgNPs

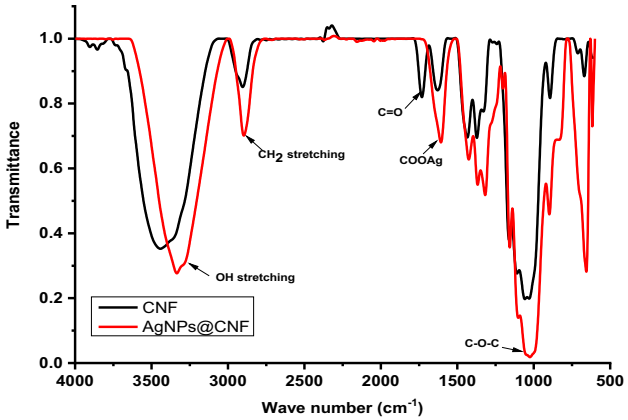

Fig. 4 FT-IR spectra of CNFs and AgNPs@CNFs

carboxylic and carbonyl groups in the oxidized nanofibrils which generate electrons needed to initiate the reduction at elevated temperatures [2, 33, 34]. The increase in the intensity of the plasmon bands is an indication of the gradual increase in the amount of AgNPs being formed in solution as silver ions are being [2]. This growth has been reported to occur via three mechanisms in which the metal ions first get adsorbed on the negatively charged CNF through electrostatic interaction or covalent bonding. In the case of transition metal cations, they undertake stronger covalent bonds with CNF as compared to the electrostatic interactions observed in alkali metal ions. Upon adsorption, the metal ions are anchored on CNF and due to the presence of C=O groups on the surface of the fibrils, they are reduced to NPS. This behavior has also been observed for other metal species such as copper and it suggests that the anchoring of the metal ions on CNFs could significantly promote their reduction[20]. This peak centered at 412 nm has also been observed when silver nanoparticles have been synthesized using different reducing agents such as secondary metabolites and is often used as a qualitative indicator of the reduction [35–38].

3.2 FTIR Characterization of AgNPs@CNFs

The FT-IR spectra of CNFs and AgNPs@CNFs are shown in Fig. 4.

The IR spectra of CNFs had similar peaks to those that have been observed in native cellulose except for the C = O functional group associated with carbonyl compounds (Fig. 4). Peaks at 3480, 2905, 1050 cm^{-1} were linked to the OH stretching vibration, CH_2 stretching vibrations and C–O–C stretching vibrations while the peak at 1722 and 1622 cm^{-1} were linked to the C=O stretching vibration of the carbonyl groups and water adsorbed on the surface that resulted from TEMPO-dialdehyde oxidation of cellulose [6, 39]. From the FT-IR spectrum of AgNPs@CNFs, it was observed that upon reduction of Ag^+ to AgNPs using CNFS, the carbonyl vibrational peak that was initially observed at 1722 cm^{-1} had shifted to 1610 cm^{-1} [21]. This shift in the carbonyl vibrational band could be attributed to the fact that the carbonyl group participated in the reduction of AgNPs and resulted in the interaction of the C=O and AgNPs hence the absence of the C=O vibrational in the spectrum of AgNPs@CNFs [13, 34]. Essentially the carbonyl is being consumed to reduce Ag ions which resulted in their absence in AgNPs@CNFs spectrum. In a typical glucose reduction of Ag ions or Tollens reaction, carbonyl of the aldehyde of the glucose, (which in this case, it is from CNF) reduce Ag ions and resulted in a formation of carboxylate group that may overlapped with the 1610 cm^{-1} peak of absorbed water. This could also explain a much intense of IR peak observed for AgNPs@CNFs in Fig. 4. Interaction of the surface OH groups with AgNPs was also observed from the shift in the OH vibrational peak which initially was centered at 3445 cm^{-1} but shifted to 3333 cm^{-1} upon introduction of AgNPs within CNFs matrix. This shift has been linked to the formation of a chemical bond or an electrostatic interaction between the AgNPs and oxygen containing functional groups present in CNFs [2]. Presence of the vibration peak of the C–O–C at 1050 cm^{-1} was also an indication that the polysaccharide structure of cellulose was sustained even after oxidation and the reduction of silver ions [21, 22]

3.3 XRD Diffractogram of CNFs and AgNPs@CNFs

The X-ray powder diffraction patterns of CNFs and AgNPs@CNFs are shown in Fig. 5.

From examination of XRD profile of CNF (Fig. 5; Table 1), it was observed that the two peaks of cellulose that are usually observed at 2θ values of 16° and 22° that

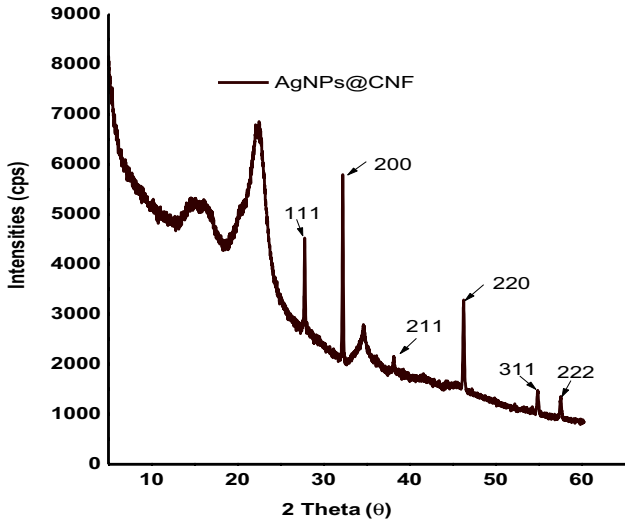

Fig. 5 Powder X-ray diffraction patterns of CNF and Ag/AgCl@CNFs

Table 1 Peak position, FWHM and crystallite size of AgNPs@CNFs

Peak position (2θ)	Crystallite size (nm)
22	2.5
28	14.4
32	7.6
46	6.7
55	4.3
57	4.8

correspond to (001) and (200) crystal planes in cellulose structure were present [14, 40, 41]. Calculation of the degree of crystallinity established that CNF had a crystallinity of 63% with a crystallite size of 2.5 nm while AgNPs had variable crystallite size (Table 1). One interesting observation was that, while periodate oxidation of native cellulose resulted in a completely amorphous dialdehyde cellulose [27], periodate oxidation of CNF did not yield an amorphous material but rather a more crystalline cellulose. TEMPO oxidation produces a crystalline cellulose which upon periodate oxidation would not amorphous material as observed in literature but crystalline cellulose since amorphous domains are subsequently removed during TEMPO oxidation. It is worth mentioning that when CNFs are subjected to periodate oxidation only, the C_2 and C_3 bond are cleaved leading to formation of an amorphous material. This change in structure is usually confirmed by the appearance of the amorphous peak centered at 2θ = 18° and the disappearance of the crystalline peaks commonly observed at 2θ values of 16° and 22°. Upon TEMPO and periodate oxidation of cellulose, the oxidized nanofibrils were used to synthesize AgNPs@CNFs. From the AgNPs@CNFs diffractograms (Fig. 5), it was observed that CNF was able to reduce Ag^+ ion in solution to AgNPs as peaks belonging to AgNPs were observed. The sharp distinct peaks observed at 2θ = 38°, 55°, and 57° have previously been indexed with (111), (200), (220) and (311) crystalline planes of face-centered cubic structure of metallic silver (JCPDS file: 65-2871) [13, 21, 22]. The peaks centered at 2θ = 28°, 32°, and 46° have been associated with presence of AgCl nanoparticles (JCPDS no. 31-1238) that are synthesized together with AgNPs and can be associated with trace amounts of chlorine present in the CNFs as a result of the solvents used. This drawback can be overcome by use of high intensity UV radiation that has been reported to reduce AgCl nanoparticles to AgNPs [36, 42]

3.4 DSC Thermograms of CNF and AgNPs@CNFs

Figures 6 shows the DSC thermograms of CNF and AgNPs@CNFs.

From Fig. 6, it can be observed that CNFs comprised of an initial endothermic peak centred at 68 ℃ an exothermic peak centred at 331 °C and a final endothermic peak centred at 416 °C. The initial endothermic peak was as a result of water adsorbed on the surface of cellulose that evaporated during the analysis while the final endothermic peak may be attributed to residual lignin which has been reported to occur at this temperature. One thing to note is that the endothermic peak of cellulose which is normally situated between 250 and 330 °C degrees was absent and this can be associated with the changes that occurred during synthesis of CNF. As for AgNPs@CNF, presence of AgNPs resulted in a shift in the peaks observed at 68 °C and 331 °C to 79 °C and 264 °C respectively. It can be noted that during synthesis the structure of cellulose undergoes changes as both oxidation process leads to introduction of carboxyl group at C_6 and dialdehyde functional groups at C_2 and C_3 of cellulose leading to cleavage of C_2–C_3 bond in cellulose [6, 27, 43].

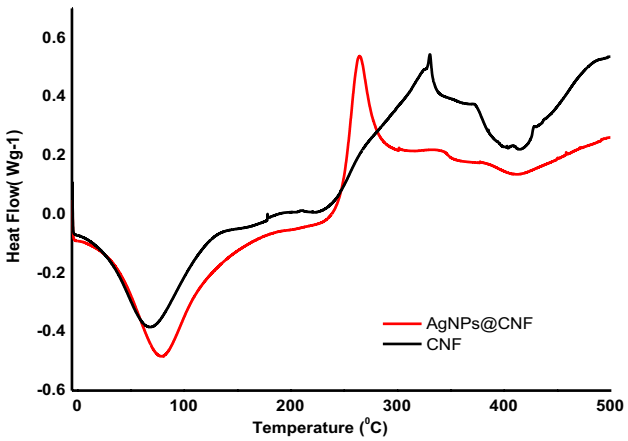

Fig. 6 DSC thermograms of CNFs and AgNPs@CNFs

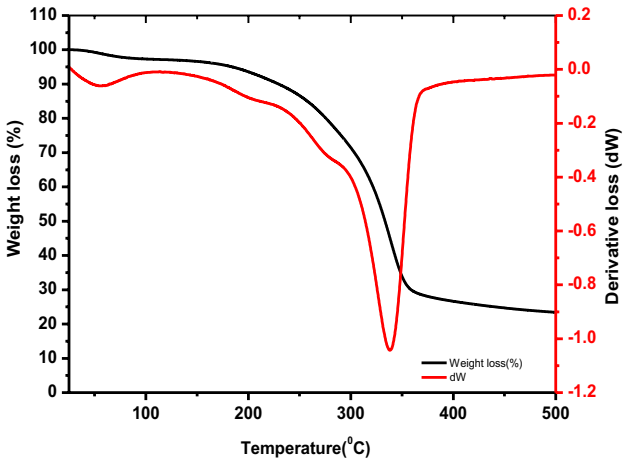

Fig. 7 TGA/DTGA curves of cellulose nanofibrils

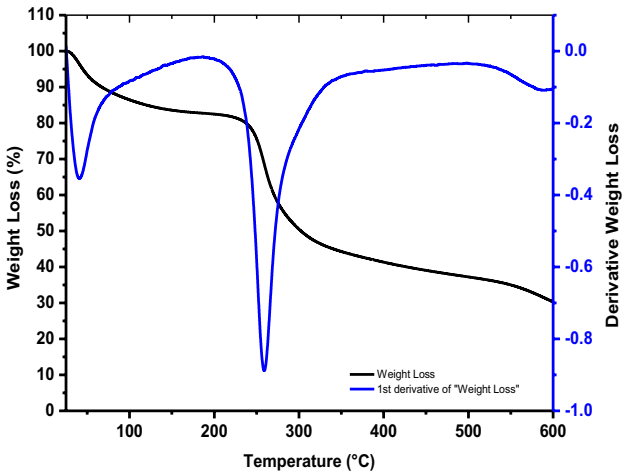

Fig. 8 TGA-DTGA thermograms of AgNPs@CNFs

3.5 TGA-DTGA Thermograms of AgNPs@CNFs

Figures 7 and 8 show TGA/DTGA thermograms of CNF and AgNPs@CNFs.

From Figs. 7 and 8, the first degradation stage of ~ 4% weight loss was associated with evaporation of water molecules adsorbed on CNF samples [13]. The second degradation stage which accounted for 80% weight loss with maximum degradation peak centered at 338 °C was attributed to degradation of cellulose. Comparison of TGA and DTGA profiles of CNF and AgNPs@CNFs revealed that the thermal stability was dependent on the chemical treatment the samples were subjected to with CNF being more thermally stable as it had a higher onset degradation temperature. AgNPs@CNFs had a lower onset degradation temperature of 140 °C as compared to CNF whose onset degradation temperature was 200 °C. Presence of AgNPs reduced the thermal stability of the nanofibrils as it was observed that the maximum degradation temperature of AgNPs@CNFs was lower as compared to that of CNF [13]. The thermal stability of a given polymers is determined by several factors which are related to the polymer structure such presence of functional groups, molecular weight, branch degree, cross-linking properties, and crystallinity [44]. Presence of intermolecular interactions such as dipole–dipole interactions and hydrogen bonding have also been reported to enhance the thermal stability of polymers such as polyamides. In this study, it can be reported that presence the disruption of hydrogen bond interactions due to the association of AgNPs with the COOH group introduced at C6 resulted in the decrease of thermal stability of AgNPs@CNF [44]. From Fig. 8, it was observed that AgNPs@CNFs had the highest degradation at 260 °C with 30% ash content, as compared to CNF which had the maximum degradation occurring at 338 °C with a 23% ash content. Presence of metallic species within the cellulose matrix has been reported to increase the residual ash content of the nanofibrils after thermal analysis [13, 22].

3.6 SEM Micrographs of AgNPs@CNFs

The SEM micrographs of AgNPs@CNFs are depicted in Fig. 9.

From Fig. 9, changes in morphology of AgNPs@CNFs can be visualized. As it can be observed, AgNPs@CNFs fiber morphology were significantly different when compared to CNF, DAC and native cellulose fibers that we have previously reported [14, 25, 26]. While CNF was composed of intertwined nanofibrils that appeared like a mesh, CNF and AgNPs@CNFs had sponge like surface that was porous [26]. On the other hand, DAC has been reported to be composed of a smooth surface with no visible nanofibrils being observed [14, 27, 39]. Presence of AgNPs within the cellulose nanofibrils was confirmed EDX micrographs which showed AgNPs peaks together with Carbon and oxygen (Fig. 10).

3.7 TEM Micrographs of AgNPs@CNFs

The TEM micrographs of AgNPs@CNFs are depicted in Fig. 11.

From Fig. 11, fiber length distribution of CNF was found to be between 50 and 400 nm in length. When compared to TOCNF, DAC and native cellulose, the length distribution was within the range of nanofibrils isolated in this study. TEMPO oxidation of cellulose nanofibrils has been reported to reduce fiber length while periodate on the other hand has little effect on the length of the nanofibrils though it removes crystalline domains present in cellulose. Presence of carbonyl functional groups in CNF implies that, when

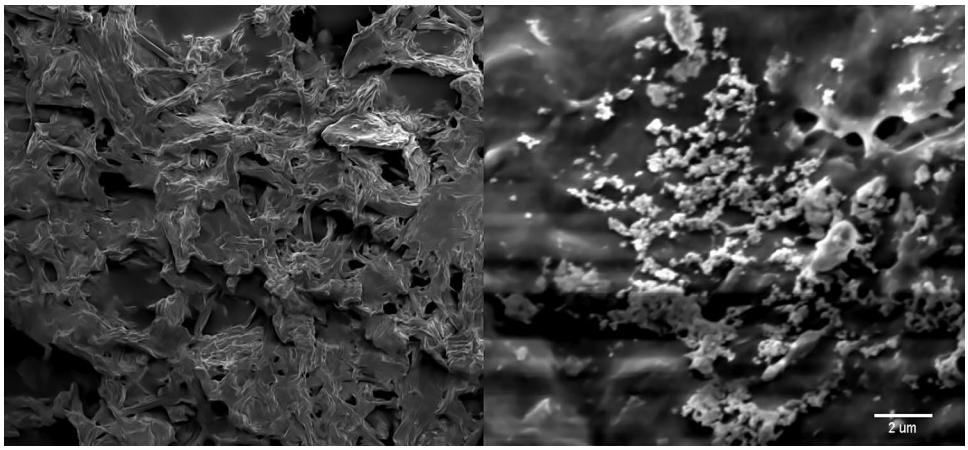

Fig. 9 SEM micrographs of AgNPs@CNFs at low and high magnification showing AgNPs on the surface of CNF

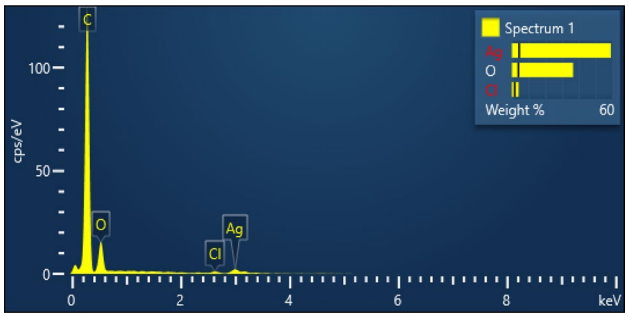

Fig. 10 EDX micrographs of AgNPs@CNFs at low and high magnification showing AgNPs on the surface of CNF

they were re-dispersed in $AgNO_3$ solution, the Ag^+ ions were reduced to AgNPs hence the observation of spherical dark particle in the TEM micrographs. These spherical dark particles were attributed to be those of AgNPs which were generated when CNF was redispersed in $AgNO_3$ solution as reported in literature [21].

3.8 Hydrodynamic Diameters of AgNPs@CNFs

The results of the zeta potential, polydispersibility index and hydrodynamic diameters of AgNPs@CNFs are depicted in Fig. 12.

From the DLS measurements obtained (Fig. 12), the average size, polydispersibility index and zeta potential of AgNPs@CNFs composite was found to be 97.8 ± 17.9 nm, 0.5393 ± 0.09 and − 23.78 ± 3.71 (mV) respectively. With the high zeta potential of AgNPs@CNFs, the tendency of this composite to aggregate was low which implied that CNF could work as a substrate for immobilizing AgNPs within the cellulose matrix to prevent their aggregation. In similar studies, the zeta potential of AgNPs@DAC and AgNPs@CNF have been reported to be − 28.8 mV and − 40.8 mV respectively [21, 22].

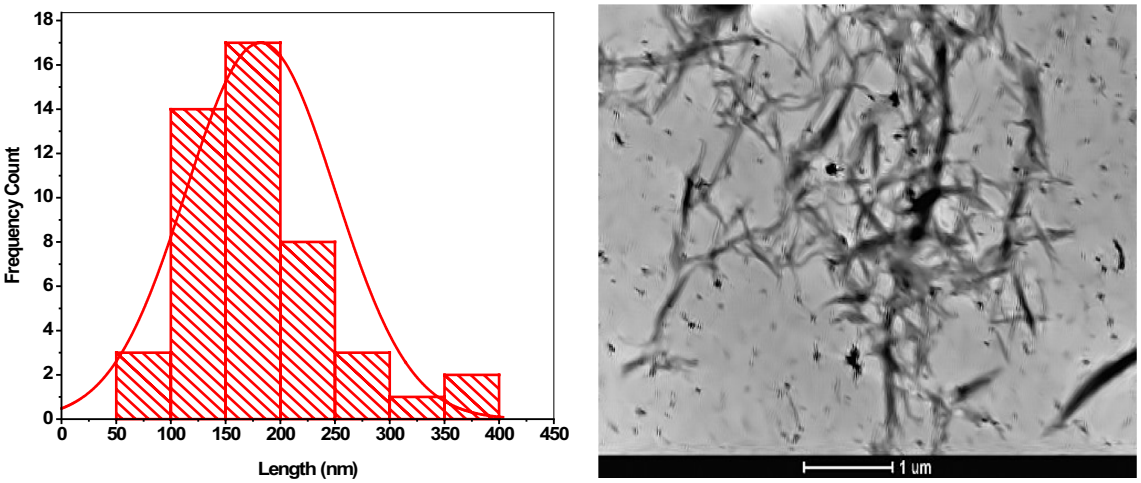

Fig. 11 TEM micrographs and size distribution of CNFs in AgNPs@CNFs composite

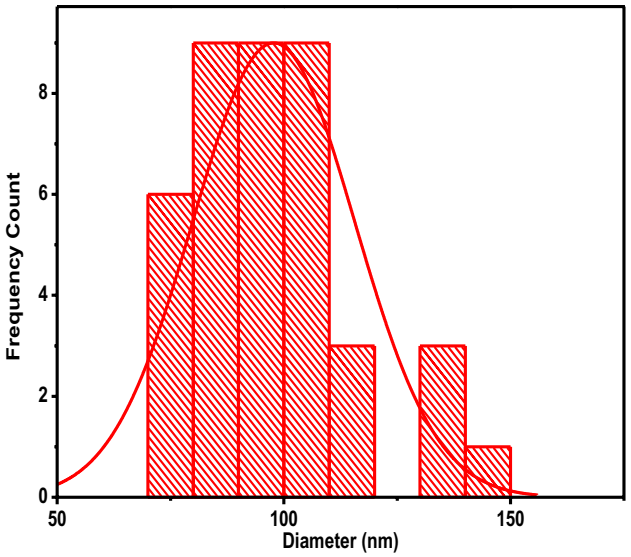

Fig. 12 Hydrodynamic diameters of AgNPs@CNFs nanocomposite

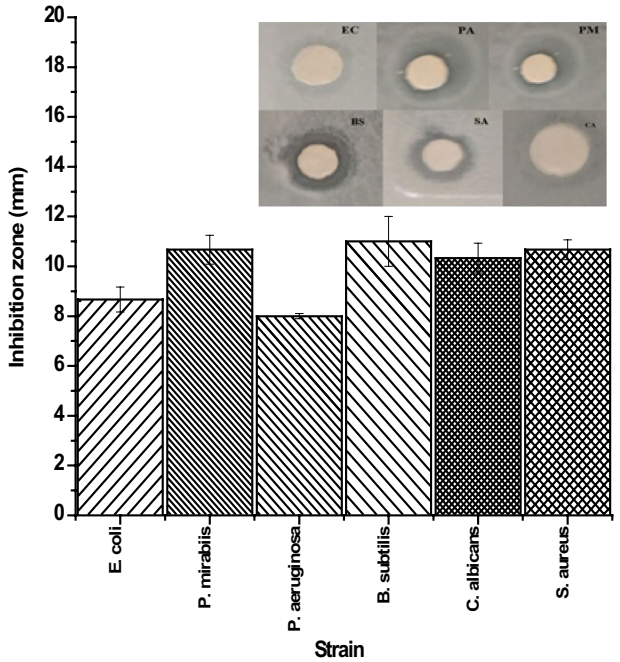

Fig. 13 Antimicrobial activity of AgNPs@CNFs against *P. aeruginosa* (PA), *E. coli* (EC), *P. mirabilis* (PM), *B. subtilis* (BS), *C. albicans mirabilis* (CA) and *S. aureus* (SA)

3.9 Antimicrobial Activity

The antimicrobial potency of AgNPs@CNFs evaluated using disc diffusion assay are depicted in Fig. 13.

After the incubation period, the antibacterial activities of the nanocomposite were carried out by measuring the inhibition zone around the disk against the selected microorganisms. The formation of a bacterial inhibition zone around the test film was used as a measure of the antibacterial activity of AgNPs@CNF as shown in Fig. 13. The AgNPs@CNFs composites displayed different antimicrobial potency against the selected microorganism but B. subtilis displayed the highest potency followed by *P. mirabilis, S. aureus*, *C. albicans*, *E. coli* and *P. aeruginosa* (Fig. 11) [2]. The differences in the antibacterial potency of the composite against the selected microorganism lies in the differences in the cell wall structure between gram-positive and gram-negative bacteria. Gram-negative bacteria contain a cell wall that is made up of multilayer structure containing a thin peptidoglycan layer, a lipoprotein layer, a lipopolysaccharide or phospholipids layer. Gram-positive bacteria on the other hand have cell walls that contain a single peptidoglycan layer that is several times thicker than that found in gram negative bacteria and they also lack an outer membrane. Due to these differences in cell wall structure, gram-positive bacteria have been found to be less susceptible to AgNPs as compared to gram negative bacteria. But in our case, AgNPs@CNF was found to be more potent to gram positive bacteria than gram negative bacteria hence the observed higher activity in *B. subtilis*, *S. aureus* and the fungi *C. albicans* [42, 45, 46]. When compared to standard antibiotics, the composite had higher antimicrobial activity as compared to standard films loaded with 10 µg of gentamycin which exhibited an inhibition zone of 13.0 ± 0, 9.0 ± 0.0, 8.0 ± 0.0 and 8.0 ± 0.0 mm for *E. coli*, *P. aeruginosa*, *S. aureus* and *B. subtilis* respectively. The disc diffusion results indicate that the nanocomposite can inhibit the growth and multiplication of *E. coli*, *P. mirabilis*, *P. aeruginosa*, *B. subtilis, S. aureus* and the fungi *C. albicans.* Previous studies have reported that the ability to inhibit cell growth is as a result of cellular deformation that results from interaction between AgNPs with the microorganisms. This interaction leads to generation of reactive oxygen species which interact with disulphide or sulfhydryl groups of enzymes thereby interrupting metabolic pathway leading to cell death [2, 5, 42].

4 Conclusion

In this work, we demonstrate that cellulose nanofibrils isolated from O. sativa can be used as a reducing agent to generate AgNPs on its surface there by imparting antimicrobial activity to the resultant nanocomposite. The in-situ generated AgNPs significantly improved the antibacterial activity of the nanocomposite against gram-positive and gram-negative bacteria and fungi. The AgNPs@CNFs nanocomposite had relatively lower thermal stability, average fibrils lengths below 400 nm and good in-vitro antimicrobial properties against selected microorganisms. The decrease in thermal stability was as a result of lower fiber lengths which meant

that heat could be easily dissipated during thermal analysis. The composite could be used as a wound dressings and packaging materials that could prevent the growth of microorganisms when applied In-vivo.

Acknowledgements The authors are grateful to the Department of Chemistry and Sino Africa Joint Research Centre-JKUAT, Jomo Kenyatta University of Agriculture and Technology for provision of facilities where part of the work was carried out. The authors also acknowledge the contribution of Dr. Jihane Hankache and Prof. Katharina M. Fromm, University of Fribourg, for granting us access to facilities used to characterize the nanocomposite.

Author Contributions EEM: Formal analysis; Investigation; Methodology; Roles/Writing—original draft; Writing—review & editing. PGK: Funding acquisition; Project administration; Resources; Supervision, Roles/Writing—original draft; Writing—review & editing. ANG: Funding acquisition; Project administration; Resources, Roles/Writing—original draft; Writing—review & editing. SMM: Writing—review & editing. DSM: Conceptualization; Data curation; Supervision; Validation.

Funding The authors also acknowledge the support of Africa-ai-Japan project 2018/2019, Kenya National Innovation Agency (KENIA) innovation Grant 2020/2021 and Research Production and Extension division (JKUAT-RPE).

Data availability Not applicable.

Code availability Not applicable.

Declarations

Conflict of interest All authors declare that they have no conflict of interest.

References

1. C. Krishnaraj, E.G. Jagan, S. Rajasekar, P. Selvakumar, P.T. Kalaichelvan, N. Mohan, Colloids Surf. B Biointerfaces **76**, 50 (2010)
2. J. Li, L. Kang, B. Wang, K. Chen, X. Tian, Z. Ge, J. Zeng, J. Xu, W. Gao, ACS Sustain. Chem. Eng. **7**, 1146 (2019)
3. M. Tavakolian, S.M. Jafari, T.G.M. van de Ven, Nano-Micro Lett. **12**, 1 (2020)
4. B. Martina, K. Kateřina, R. Miloslava, G. Jan, M. Ruta, Adv. Polym. Technol. **28**, 199 (2009)
5. S.-L. Abram, K.M. Fromm, Chem. A Eur. J. Chem. **26**, 202002143 (2020)
6. E. Hoglund, http://kau.diva-portal.org (2015)
7. Y. Zhou, T. Saito, L. Bergstrom, A. Isogai, Biomacromol **19**, 633 (2018)
8. M. Le Gars, A. Delvart, P. Roger, M.N. Belgacem, J. Bras, Colloid Polym. Sci. **298**, 603 (2020)
9. H. Ghasemzadeh, A. Mahboubi, K. Karimi, S. Hassani, Polym. Adv. Technol. **27**, 1204 (2016)
10. S.L. Arias, A.R. Shetty, A. Senpan, M. Echeverry-Rendón, L.M. Reece, J.P. Allain, J. Vis. Exp. **2016**, 52951 (2016)
11. N. Barrera, L. Guerrero, A. Debut, P. Santa-Cruz, PLoS ONE **13**, e0200918 (2018)
12. Y. Xu, S. Li, X. Yue, W. Lu, BioResources **13**, 2150 (2018)
13. G. Wang, F. Li, L. Li, J. Zhao, X. Ruan, W. Ding, J. Cai, A. Lu, Y. Pei, ACS Omega **5**, 8839 (2020)
14. E.S. Madivoli, P.G. Kareru, A.N. Gachanja, S.M. Mugo, D.S. Makhanu, SN Appl. Sci. **1**, 1 (2019)
15. P. Liu, B. Pang, S. Dechert, X.C. Zhang, L.B. Andreas, S. Fischer, F. Meyer, K. Zhang, Angew. Chem. Int. Ed. **59**, 3218 (2020)
16. S. Thiangtham, J. Runt, H. Manuspiya, Carbohydr. Polym. **208**, 314 (2019)
17. A. Isogai, Proc. Jpn. Acad. Ser. B Phys. Biol. Sci. **94**, 161 (2018)
18. J. Henschen, P.A. Larsson, J. Illergård, M. Ek, L. Wågberg, Colloids Surf. B Biointerfaces **151**, 224 (2017)
19. N. Fiol, M.G. Vásquez, M. Pereira, Q. Tarrés, P. Mutjé, M. Delgado-Aguilar, Cellulose **26**, 903 (2019)
20. L. Valencia, S. Kumar, E.M. Nomena, G. Salazar-Alvarez, A.P. Mathew, ACS Appl. Nano Mater. **3**, 7172 (2020)
21. Q. Xu, L. Jin, Y. Wang, H. Chen, M. Qin, Cellulose **26**, 1309 (2019)
22. H. Ito, M. Sakata, C. Hongo, T. Matsumoto, T. Nishino, Nanocomposites **4**, 167 (2018)
23. C. Ponce, J. Chanona, V. Garibay, E. Palacios, G. Calderon, R. Sabo, Microsc. Microanal. **19**, 200 (2013)
24. E.S. Madivoli, P.G. Kareru, A.N. Gachanja, S.M. Mugo, M.K. Murigi, P.K. Kairigo, K. Cheruiyot, J.K. Mutembei, F.K. Njonge, Int. Res. J. Pure Appl. Chem. **12**, 1 (2016)
25. M.K. Murigi, E.S. Madivoli, M.M. Mathenyu, P.G. Kareru, A.N. Gachanja, P.K. Njenga, G. Nowsheen, P.N. Githira, M. Githua, IOSR J. Polym. Text. Eng. **1**, 53 (2014)
26. E.S. Madivoli, P.G. Kareru, A.N. Gachanja, S.M. Mugo, D.M. Sujee, K.M. Fromm, J. Nat. Fibers **5**, 1 (2020)
27. J. Leguy, A. Diallo, J.L. Putaux, Y. Nishiyama, L. Heux, B. Jean, Langmuir **34**, 11066 (2018)
28. Y. Chen, Q. Wu, B. Huang, M. Huang, X. Ai, BioResources **10**, 684 (2014)
29. M. Jonoobi, J. Harun, A.P. Mathew, M.Z.B. Hussein, K. Oksman, Cellulose **17**, 299 (2010)
30. L.K. Kian, M. Jawaid, H. Ariffin, O.Y. Alothman, Int. J. Biol. Macromol. **103**, 931 (2017)
31. D. Ciolacu, F. Ciolacu, V.I. Popa, Cellul. Chem. Technol. **45**, 13 (2011)
32. Y.Y. Loo, Y. Rukayadi, M.-A.-R. Nor-Khaizura, C.H. Kuan, B.W. Chieng, M. Nishibuchi, S. Radu, Front. Microbiol. **9**, 1555 (2018)
33. A. Errokh, A. Magnin, J.L. Putaux, S. Boufi, Cellulose **25**, 3899 (2018)
34. A. Errokh, A. Magnin, J.L. Putaux, S. Boufi, Mater. Sci. Eng. C **105**, 1 (2019)
35. S. Akmaz, E. Dilaver Adiguzel, M. Yasar, O. Erguven, Adv. Mater. Sci. Eng. **2013**, 1 (2013)
36. S.I. Vasylevskyi, S. Kracht, P. Corcosa, K.M. Fromm, B. Giese, M. Füeg, Angew. Chem. Int. Ed. **56**, 5926 (2017)
37. I.-M. Chung, I. Park, K. Seung-Hyun, M. Thiruvengadam, G. Rajakumar, Nanoscale Res. Lett. **11**, 40 (2016)
38. X.C. Jiang, W.M. Chen, C.Y. Chen, S.X. Xiong, A.B. Yu, Nanoscale Res. Lett. **6**, 1 (2011)
39. J. Leguy, *Periodate Oxidation of Cellulose for Internal Plasticization and Materials Design* (Doctoral dissertation. Université Grenoble Alpes, 2018)
40. I. Besbes, M.R. Villar, S. Boufi, Carbohydr. Polym. **86**, 1198 (2011)
41. M. Poletto, O.J. Heitor, A.J. Zattera, Materials (Basel) **7**, 6105 (2014)
42. M.R. Khan, K.M. Fromm, T.F. Rizvi, B. Giese, F. Ahamad, R.J. Turner, M. Fueg, E. Marsili, Part. Part. Syst. Charact. **37**, 1900419 (2020)
43. J. Wei, C. Du, H. Liu, Y. Chen, H. Yu, Z. Zhou, BioResources **11**, 8386 (2016)

44. N.Z. Tomić, in *Compatibilization of Polymer Blends: Micro and Nano Scale Phase Morphologies Interphase Characterization and Properties*. ed. by S. Thomas (Elsevier, Amsterdam, 2019), pp. 489–510
45. Z. Wu, W. Deng, J. Luo, D. Deng, Carbohydr. Polym. **205**, 447 (2019)
46. A. Azam, A.S. Ahmed, M. Oves, M.S. Khan, S.S. Habib, A. Memic, Int. J. Nanomed. **7**, 6003 (2012)